Available online at www.sciencedirect.com
SCIENCE DIRECT®
Journal of Solid State Chemistry 174 (2003) 285–295
JOURNAL OF SOLID STATE CHEMISTRY
http://elsevier.com/locate/jssc

Structural relations between weberite and zirconolite polytypes—refinements of doped 3T and 4M $Ca_2Ta_2O_7$ and 3T $CaZrTi_2O_7$

I.E. Grey,[a,*] W.G. Mumme,[a] T.J. Ness,[b] R.S. Roth,[c] and K.L. Smith[d]

[a] *CSIRO Minerals, Box 312, Clayton South, Victoria 3169, Australia*
[b] *Department of Chemistry, Monash University, Clayton, Victoria 3168, Australia*
[c] *National Institute of Standards and Technology, Gaithersburg, MD 20899, USA*
[d] *Australian Nuclear Science and Technology Organisation, Menai NSW 2234, Australia*

Received 19 December 2002; received in revised form 30 March 2003; accepted 17 April 2003

Abstract

New weberite-type $Ca_2Ta_2O_7$ and zirconolite-type $CaZrTi_2O_7$ polytypes have been prepared by doping with Nd/Zr and Th/Al, respectively, and their structures have been refined using single-crystal X-ray diffraction intensity data. The 3T zirconolite polytype, $Ca_{0.8}Ti_{1.35}Zr_{1.3}Th_{0.15}Al_{0.4}O_7$, has $a = 7.228(1)$, $c = 16.805(1)$ Å. The 3T weberite-type polytype, $Ca_{1.92}Ta_{1.92}Nd_{0.08}Zr_{0.08}O_7$, has $a = 7.356(1)$, $c = 18.116(1)$ Å. Both 3T polytypes have space group $P3_121$, $Z = 6$. The 4M $Ca_2Ta_2O_7$ polytype has the same composition, from electron microprobe analyses, as the 3T polytype, and has cell parameters: $a = 12.761(1)$, $b = 7.358(1)$, $c = 24.565(1)$ Å, $\beta = 100.17(1)°$, space group $C2$, $Z = 16$. The structural relationships between the different zirconolite and weberite polytypes are discussed. A consideration of the structures from the viewpoint of anion-centered tetrahedral arrays shows that zirconolite can be considered as an anion-deficient fluorite derivative phase. However, the fluorite-type topology of edge-shared OM_4 tetrahedra is not maintained in the $Ca_2Ta_2O_7$ weberite-type polytypes, even though they have a fluorite-like *fcc* packing of metal atoms. One of the oxygen atoms moves from a tetrahedral Ta_3Ca interstice to an adjacent Ta_2Ca_4 octahedral interstice in the weberite polytypes.

1. Introduction

Zirconolite and weberite minerals and related synthetic phases have in common the general formula M_4X_7 and anion-deficient fluorite-type structures. Weberite is the name originally given to a fluoride mineral of composition Na_2MgAlF_7 [1], with orthorhombic symmetry. Its structure can be described in terms of cubic stacking of two types of close-packed metal atom layers parallel to $(111)_{fluorite}$, having alternately the compositions Mg_2AlNa and Na_3Al. In the first type of layer the small cations form hexagonal tungsten bronze type (HTB) arrays of corner-connected octahedra with 8-coordinated Na atoms in the hexagonal rings. The second type of layer is made of kagome nets of Na atoms with Al in the hexagonal rings. The Na atoms have distorted cubic coordination and the Al is octahedrally coordinated. The polyhedra are interconnected by edge-sharing. The octahedra in the two types of layers are corner-connected, giving a three dimensional framework of composition $[MgAlF_7]^{2-}$. In the Mg_2AlNa layers, *trans*-connected $[MgF_5]$ octahedral chains alternate with chains containing AlF_6 octahedra and NaF_8 hexagonal bipyramids. A number of different weberite fluoride polytypes have been characterized which have the above structural features in common, and differ only in the relative orientations of the $[M^{2+}F_5]$ chains in successive $M_2^{2+}M^{3+}Na$ layers [2].

Weberite structures have also been characterized in oxide systems including antimonates [3], osmates [4] and tantalates [5,6]. In contrast to the fluorides, which are all ternary phases, the oxide weberites are usually binary phases of general composition $A_2B_2O_7$, A = large cations (Ca, Cd, Sr, etc.) and B = small cations (Sb, Os, Ta). As for the fluorides, their structures comprise an alternation of $(111)_{fluorite}$ closest-packed metal atom layers with compositions A_3B and B_3A. A number of different oxide

*Corresponding author. Fax: +613-9562-8919.
E-mail address: ian.grey@csiro.au (I.E. Grey).

0022-4596/03/$ - see front matter © 2003 Elsevier Inc. All rights reserved.
doi:10.1016/S0022-4596(03)00222-6

weberite polytypes are known. These can be distinguished by using the nomenclature of the IMA New Minerals and Mineral Names Pyrochlore Subcommittee [7]. This gives the number of double layers ($A_3B + B_3A$) in the unit cell followed by a letter indicating the symmetry. For example weberite itself is a 2O polytype. Other structurally characterized weberite polytypes include 2M, 4M and 3T [2] and 6T [6].

Zirconolite, ideally $CaZrTi_2O_7$, also has a fluorite-type *fcc* packing of metal atoms [8], and an alternation of two compositionally distinct metal atom layers. However, the metal layer compositions, Ca_2Zr_2 and Ti_4, are different to those in weberites. In the large-cation layers, rows of CaO_8 cubes alternate with rows of ZrO_7 mono-capped octahedra. In the Ti_4 layer, both the nodes of the kagome net of octahedra and the hexagonal rings are occupied by Ti. The Ti is displaced from the center of the ring to take up 4- or 5-coordination. The aristotype zirconolite is a 2M polytype [9]. Other zirconolite polytypes reported are 3T and 3O [10], 6T [11] and 4M [12]. The different polytypes are distinguished by the relative orientations of the rows of edge-shared CaO_8 cubes in successive large-cation layers.

The relationships of the weberite and zirconolite structures to the $A_2B_2X_7$ pyrochlore structure have separately been discussed, but their relationships to one another have not been analyzed. We have carried out structure refinements of 3T polytypes of both zirconolite (doped with Th and Al) and weberite ($Ca_2Ta_2O_7$ doped with Nd and Zr), and have determined the structure of a new 4M $Ca_2Ta_2O_7$ weberite polytype. Despite being the simplest (smallest cell) of the $Ca_2Ta_2O_7$ polytypes, the structure of the 3T polytype has not been previously reported, due to the difficulty of obtaining single crystals [5]. Only one structure determination of 3T zirconolite has been reported [10]. The quality of the structure analysis was hampered because the crystal contained two other polytypes, intergrown with the 3T component. The structure results on 3T and 4M weberite calcium tantalates and 3T zirconolite are reported here, together with a discussion of the structural relationships between the two mineral types.

2. Experimental

2.1. Syntheses

The 3T zirconolite polytype was prepared during a systematic study of the effect of different dopant elements on the stability of zirconolite phases [11]. A mixture of oxides corresponding to the composition $Ca_{0.75}Ti_{1.5}ZrTh_{0.25}Al_{0.5}O_7$ was pressed into a pellet and heated at 1510°C for 10 days then at 1520°C for 5 days. The sintered product comprised interlocking clear crystals, some hundreds of micrometres in size. The structure and compositions of selected crystals were checked using a JEOL 2000FXII TEM fitted with a Link ISIS energy dispersive X-ray spectrometer. The *k*-factors required as input for quantitative thin film analysis were determined from a range of synthetic and natural materials as described by Lumpkin et al. [13]. The structure of the crystals analyzed was pure 3T zirconolite, with some fragments displaying stacking faults. The analyses gave 12.4 wt% CaO, 29.6 wt% TiO_2, 42.5 wt% ZrO_2, 9.5 wt% ThO_2 and 6.4 wt% Al_2O_3. The analyses are accurate to 0.2–0.5 oxide wt%. The charge-balanced M_4O_7 composition $Ca_{0.8}Ti_{1.35}Zr_{1.3}Th_{0.15}Al_{0.4}O_7$ gives a reasonable fit to the experimental analyses (calculated 12.0 wt% CaO, 28.9 wt% TiO_2, 42.9 wt% ZrO_2, 10.6 wt% ThO_2 and 5.5 wt% Al_2O_3).

The new calcium tantalate polytypes were prepared as part of a work program [5] on the effect of different dopant elements on the stability of phases in the system $CaO–Ta_2O_5$ + dopants. The crystals used in this study were prepared from a mixture of oxides corresponding to the composition $(Ca_2Ta_2O_7)_{0.8}(Nd_2Zr_2O_7)_{0.2}$. An equal weight of $Ca_2B_2O_5$ as flux was added to the synthetic composition and the mixture was heated in a sealed platinum tube at 1450°C for 2 h, then cooled to 1000°C at 1°/h before removing from the furnace. The excess flux was removed by washing with dilute HCl. The product contained two different types of colorless crystals, in the form of elongated laths with rectangular cross-section and trigonal pyramids. From precession photographs, these were identified as 3T (trigonal) and 4M (monoclinic) polytypes, respectively.

Wavelength-dispersive electron microprobe analyses were made on the crystals using a JEOL Superprobe operated at 15 kV and using NdF_3, $ZrSiO_4$ and $CaTa_2O_6$ as standards. Within the analysis variations on different crystals (0.1–0.2 wt% oxides), the same results were obtained for the 3T and 4M crystals. The average of 4 analyses gave 20.3 wt% CaO, 74.5 wt% Ta_2O_5, 1.9 wt% ZrO_2 and 2.5 wt% Nd_2O_3. These analyses depart slightly from a charge balanced M_4O_7 formula (charge balance gives $M_4O_{6.9}$), probably due to matrix correction errors. On the basis that the formula conforms to M_4O_7, the composition $Ca_{1.92}Ta_{1.92}Nd_{0.08}Zr_{0.08}O_7$ (calculated 19.4 wt% CaO, 76.4 wt% Ta_2O_5, 1.8 wt% ZrO_2 and 2.4 wt% Nd_2O_3) gives a reasonable fit to the experimental results.

2.2. Single-crystal structure studies

The precession method was used to check the quality of the crystals and identify the symmetry and polytype. Intensity data collections were then made using a Nonius Kappa diffractometer employing a CCD area detector. The data collection conditions are given in Table 1. The CCD intensity data sets were processed to produce absorption-corrected data files, which were

Table 1
Summary of data collection conditions and refinement parameters

	3T zirconolite	3T weberite	4M weberite
Formula (microprobe)	$Ca_{0.8}Ti_{1.35}Zr_{1.3}Th_{0.15}Al_{0.4}O_7$	$Ca_{1.92}Ta_{1.92}Nd_{0.08}Zr_{0.08}O_7$	$Ca_{1.92}Ta_{1.92}Nd_{0\cdot08}Zr_{0.08}O_7$
Crystal data			
Cell parameters	$a = 7.228(1)$ $c = 16.805(1)$ Å	$a = 7.356(1)$ $c = 18.116(1)$ Å	$a = 12.761(1)$, $b = 7.358(1)$ $c = 24.565(1)$ Å, $\beta = 100.17(1)^\circ$
Z	6	6	16
Space group	$P3_121$	$P3_121$	$C2$
Data collect			
Temperature (K)	123	123	295[a]
λ (Mo$K\alpha$)	0.71073	0.71073	0.71073
Crystal size (mm)	$0.18 \times 0.13 \times 0.050$	$0.10 \times 0.05 \times 0.05$	$0.07 \times 0.05 \times 0.025$
Collection mode	As for weberite	ϕ scan, 0–360°, $\Delta\phi = 1^\circ$	ϕ scan, 0–360°, $\Delta\phi = 0.5^\circ$
Count time per frame	45 s	45 s	100 s
2θ max (deg)	60	60	60
Reflection range	$-10 \leqslant h$, $k \leqslant 10$; $-20 \leqslant l \leqslant 19$	$-10 \leqslant h$, $k \leqslant 10$; $-24 \leqslant l \leqslant 25$	$-17 \leqslant h \leqslant 17$, $-10 \leqslant k \leqslant 10$, $-34 \leqslant l \leqslant 34$
Total no. reflections	10,990	12,180	15,454
No. unique reflections	1420	1663	5822
No. reflections, $F > 4\sigma(F)$	1223	1582	5332
Absorption correction	$\mu = 10.0\,mm^{-1}$	$\mu = 38.7\,mm^{-1}$	$\mu = 38.7\,mm^{-1}$
(Empirical)	$T_{min} = 0.58$, $T_{max} = 0.86$	$T_{min} = 0.12$, $T_{max} = 0.20$	$T_{min} = 0.57$, $T_{max} = 0.70$
R (merge) on F^2	0.05	0.05	0.05
Refinement			
Parameters refined	57	50	182
w$R_2(F^2)$, all data	0.13	0.11	0.15
$R_1, F > 4\sigma(F)$	0.051	0.032	0.056
R_1, all data	0.062	0.038	0.064
GOF	1.14	1.52	1.15

[a] Low temperature facility not available for this data collect.

used with SHELXL [14] for the structure determinations and refinements.

3*T zirconolite*. The coordinates for 3T zirconolite [10] were used to initiate the refinement in $P3_121$, which converged using major element site assignments (Ca, Zr and Ti) to a high R_1 value of 0.18. Thermal parameters and difference Fourier maps were used to help identify the sites containing the minor substituents, Th and Al. Introduction of Th in the calcium sites gave a marked improvement in the fit to the experimental intensity data. The possibility of more than two different metal atoms occupying each of the metal atom sites can lead to ambiguity in the site occupancies obtained by refinement. Use was made of published studies of site occupancy refinements of Zr-rich zirconolite $CaZr_xTi_{3-x}O_7$ with $x > 1$, which concluded that excess Zr is incorporated in both the Ti sites and the Ca sites [9,15]. The excess Zr in the 3T phase was distributed uniformly between the Ti and Ca sites. The Al/Ti distributions were then refined in the Ti sites and the Ca/Th distributions were refined in the Ca sites. One of the Ti sites was found to be split into two distinct sites, $M(5)$ and $M(5)'$ in Table 2, with 5- and 4-coordination to oxygen, respectively. The coordinates for the $M(5)$ and $M(5)'$ sites were refined independently but the thermal parameters were constrained to be equal and the site occupation factors were linked in the refinement so that their sum corresponded to full occupancy of a single site. The 4-coordinated site was constrained to contain only Al, and Ti/Zr were placed in the 5-coordinated site. The final refinement, involving 57 coordinates, site occupation factors and isotropic thermal parameters, converged at $R_1 = 0.051$ for 1223 observed reflections. The refinement details are given in Table 1. The structure parameters from the refinement are reported in Table 2.

3*T calcium tantalate*. The coordinates for 3T Na_2MnFeF_7 [16] were used to initiate the refinement in $P3_121$, with Ca in the Na sites and Ta in the Mn and Fe sites. The refinement proceeded smoothly to an R_1 value of 0.05. Low thermal parameters for two of the Ca atoms and high thermal parameters for two of the Ta atom sites provided evidence for substitution of the minor components Nd and Zr. Different refinements were conducted in which mixed occupancy of these sites was allowed. The final refinement, involving 50 coordinates, site occupation factors and isotropic thermal parameters, converged at 0.032 for 1582 observed reflections with $F > 4\sigma(F)$. The refinement details are given in Table 1. The refined structure parameters are reported in Table 2.

Table 2
Refined structure parameters for the 3T polytypes

Site	Metal site occupancies	x	y	z	U (Å^2)
3T zirconolite					
$M(1)$	0.420(2) Ca + 0.020(2) Th + 0.06 Zr	0.8325(2)	0	1/3	0.0071(5)
$M(2)$	0.309(3) Ca + 0.131(3) Th + 0.06 Zr	0.3342(2)	0	1/3	0.0096(3)
$M(3)$	0.96(2) Zr + 0.04(2) Ca	0.1647(1)	0.6633(1)	0.01782(4)	0.0071(3)
$M(4)$	0.22(2) Ti + 0.22(2) Al + 0.06 Zr	0.3291(4)	0	5/6	0.0063(4)
$M(5)$	0.26(1) Ti + 0.06 Zr	0.9217(7)	0.050(1)	0.8319(3)	0.016(1)
$M(5)'$	0.18(1) Al	0.917(4)	0.110(5)	0.833(1)	0.016(1)
$M(6)$	0.82(3) Ti + 0.08(3) Al + 0.10 Zr	0.4995(3)	0.3323(4)	0.16426(7)	0.0085(5)
O(1)		0.600(1)	0.629(1)	0.1450(4)	0.019(1)
O(2)		0.007(1)	0.828(1)	0.0669(3)	0.012(1)
O(3)		0.526(1)	0.305(1)	0.0469(3)	0.007(1)
O(4)		0.192(1)	0.218(1)	0.1458(3)	0.012(1)
O(5)		0.525(1)	0.889(1)	0.0546(3)	0.009(1)
O(6)		0.939(1)	0.309(10)	0.0548(3)	0.008(1)
O(7)		0.211(1)	0.616(1)	0.1395(4)	0.015(1)
3T weberite (calcium tantalate)					
$M(1)$	0.485(3) Ca + 0.015 Nd	0.8412(5)	0	1/3	0.0080(9)
$M(2)$	0.5Ta	0.31000(7)	0	1/3	0.0052(2)
$M(3)$	0.968(6) Ca + 0.032 Nd	0.1594(5)	0.6475(3)	0.0038(1)	0.0111(7)
$M(4)$	0.46 Ta + 0.03 Zr + 0.01 Nd	0.32910(7)	0	5/6	0.0049(2)
$M(5)$	0.5Ca	0.8333(7)	0	5/6	0.0115(7)
$M(6)$	0.93 Ta + 0.05 Zr + 0.02 Nd	0.5019(1)	0.33232(6)	0.16285(2)	0.0042(1)
O(1)		0.557(1)	0.606(1)	0.1994(4)	0.015(1)
O(2)		0.957(1)	0.802(1)	0.0484(4)	0.012(1)
O(3)		0.547(1)	0.406(1)	0.0574(3)	0.011(1)
O(4)		0.201(1)	0.223(1)	0.1488(4)	0.016(1)
O(5)		0.542(1)	0.789(1)	0.0646(3)	0.014(1)
O(6)		0.963(1)	0.312(1)	0.0572(3)	0.010(1)
O(7)		0.198(1)	0.634(1)	0.1519(4)	0.013(1)

4*M calcium tantalate*. The refined cell parameters for the *C*-centered monoclinic cell are given in Table 1. The systematic extinctions were consistent with space groups *C*2/m, *C*2 or *C*m. The structural systematics observed in other weberite polytypes were used to help establish a starting model. In particular, we have noted that the relative positions of successive large-cation layers, A_3B, remain unchanged in all weberite polytypes as well as in pyrochlore [6]. The problem of determining the cation ordering in a particular polytype then reduces to determining the relative locations of the large A atoms in the B_3A layers. This was done for the 4M polytype by working in triclinic *C*1 symmetry (to avoid space group bias) and testing all possible relative locations of the Ca atom in each of the four separate $CaTa_3$ layers. The oxygen atoms were not considered at this stage and ideal coordinates for the metal atoms were used, based on cubic close packing.

The models were checked by fitting low-angle ($\sin\theta/\lambda < 0.4$) reflection data, for which the approximation of ideal coordinates did not affect the intensities significantly. The metal atom ordering that gave the lowest R factor conformed to the space group *C*2. The metal atom coordinates for this model were then refined in *C*2 and the oxygen atoms were located in difference Fourier maps. Different refinements were then conducted involving substitution of the minor elements Nd and Zr in the different sites, using the thermal parameters as a guide as to which sites the substitutions occurred. The refinements were relatively insensitive to the minor element substitutions. The final refinement, of 182 coordinates, site occupancies and isotropic thermal parameters converged at $R_1 = 0.056$ for 5332 observed reflections. The refinement details are given in Table 1 and the refined parameters are reported in Table 3.

3. Results and discussion

3.1. 3T zirconolite

The metal atom ordering in 3T zirconolite is illustrated in Fig. 1(a). It is seen that there is an alternation of two types of layers normal to the *c*-axis. One of the layers has the ideal composition Ti_4 and comprises a kagome net of titanium atoms, Ti_3, with a statistical distribution of small cations in positions displaced from the centers of the hexagonal rings.

Table 3
Refined structure parameters for 4M weberite (calcium tantalate)

Site	Metal site occupancies	x	y	z	U (Å^2)
Ca(1)	0.5 Ca	0	0	0	0.027(2)
Ta(1)	0.5 Ta	0	0.483(1)	0	0.0023(2)
Ca(11)	0.958(6) Ca + 0.042 Nd	0.2565(3)	0.267(1)	0.0067(2)	0.006(1)
Ta(2)	0.946(8) Ta + 0.054 Zr	0.1261(1)	0.753(1)	0.12174(4)	0.0038(2)
Ca(2)	1.0 Ca	0.1293(5)	0.269(1)	0.1287(3)	0.021(1)
Ta(21)	0.974(9) Ta + 0.026 Zr	0.3776(1)	0.007(1)	0.12772(3)	0.0050(2)
Ta(22)	0.976(8) Ta + 0.024 Zr	0.3801(1)	0.510(1)	0.12553(4)	0.0048(2)
Ca(3)	0.918(9) Ca + 0.082 Nd	0.2585(2)	0.5071(9)	0.2472(1)	0.006(1)
Ta(3)	1.0 Ta	0.2395(1)	0.017(1)	0.24980(3)	0.0064(2)
Ca(31)	1.0 Ca	0.0097(3)	0.255(1)	0.2549(2)	0.0021(8)
Ca(32)	1.0 Ca	0.0084(4)	0.745(1)	0.2504(2)	0.015(1)
Ta(4)	0.958(6) Ta + 0.042 Zr	0.1283(1)	0.505(1)	0.37414(3)	0.0046(2)
Ca(4)	0.876(8) Ca + 0.124 Nd	0.1278(2)	0.005(1)	0.3801(1)	0.0086(9)
Ta(41)	1.0 Ta	0.3790(1)	0.256(1)	0.37435(4)	0.0044(2)
Ta(42)	0.851(8) Ta + 0.149 Zr	0.3770(1)	0.754(1)	0.37134(4)	0.0044(2)
Ca(5)	0.5 Ca	0	0.512(1)	1/2	0.024(2)
Ta(5)	0.5 Ta	0	0.011(1)	1/2	0.0034(2)
Ca(51)	0.924(8) Ca + 0.076 Nd	0.2483(4)	0.258(1)	0.4985(2)	0.008(1)
O(1)		0.640(1)	0.996(2)	0.4566(6)	0.013(3)
O(2)		0.415(1)	0.484(2)	0.2068(5)	0.008(2)
O(3)		0.392(1)	0.010(2)	0.0481(5)	0.010(2)
O4)		0.137(1)	0.008(2)	0.4681(5)	0.011(2)
O(5)		0.366(1)	0.016(2)	0.2062(5)	0.009(2)
O(6)		0.125(1)	0.996(2)	0.2898(5)	0.012(2)
O(7)		0.736(1)	0.798(2)	0.3877(6)	0.018(2)
O(8)		0.171(1)	0.235(2)	0.2136(5)	0.013(3)
O(9)		0.332(1)	0.196(2)	0.2967(6)	0.011(2)
O(10)		0.086(1)	0.696(2)	0.0437(7)	0.018(3)
O(11)		0.431(1)	0.304(2)	0.4545(6)	0.008(3)
O(12)		0.590(1)	0.801(2)	0.0371(6)	0.006(3)
O(13)		0.526(1)	0.801(2)	0.3588(5)	0.013(3)
O(14)		0.855(1)	0.501(1)	0.3977(5)	0.016(2)
O(15)		0.731(1)	0.427(2)	0.1022(6)	0.017(3)
O(16)		0.823(1)	0.757(2)	0.1146(5)	0.013(2)
O(17		0.827(1)	0.307(2)	0.2915(5)	0.008(3)
O(18)		0.731(1)	0.058(2)	0.1369(5)	0.008(2)
O(19)		0.934(1)	0.258(2)	0.1374(5)	0.012(2)
O(20)		0.734(1)	0.206(2)	0.3879(6)	0.013(3)
O(21)		0.435(1)	0.705(2)	0.4510(6)	0.019(3)
O(22)		0.898(1)	0.002(2)	0.3497(5)	0.016(2)
O(23)		0.672(1)	0.321(2)	0.2024(5)	0.008(3)
O(24)		0.121(1)	0.504(2)	0.2931(5)	0.010(2)
O(25)		0.838(10	0.033(2)	0.0437(5)	0.015(3)
O(26)		0.525(1)	0.095(2)	0.1491(5)	0.012(3)
O(27)		0.525(1)	0.207(2)	0.3628(5)	0.013(3)
O(28)		0.524(1)	0.458(2)	0.1111(5)	0.013(3)

Octahedral coordination of the Ti atoms of the kagome net gives a HTB array as shown in Fig. 2(a). The other layer has ideal composition Ca_2Zr_2 and is composed of alternating chains, Ca_2 and Zr_2 of zirconium and calcium atoms. Fig. 1(a) shows that in successive Ca_2Zr_2 layers the chains are oriented at 120° to one another, parallel to [100], [010] and [110]. The Zr atoms are 7-coordinated by oxygen as deformed mono-capped octahedra (cubes with one corner removed) and the Ca atoms have distorted cubic coordination, as illustrated in Fig. 2(b).

In the zirconolite synthesis for this study, the 3T polytype was stabilized relative to the more common 2M polytype by incorporation of minor amounts of both Al and Th. The site occupancy refinements confirmed that Th substitutes in the Ca sites $M(1)$ and $M(2)$, as found also by Rossell [17] in refinements of doped 2M zirconolite. Aluminum substitutes for Ti in $M(4)$ and $M(6)$ and also occupies a tetrahedral site $M(5)'$ in the hexagonal rings of the HTB layer, see Fig. 2(a). The analyses calculated from the site occupancies in Table 2 are 11.6 wt% CaO, 28.0 wt% TiO_2, 43.1 wt% ZrO_2,

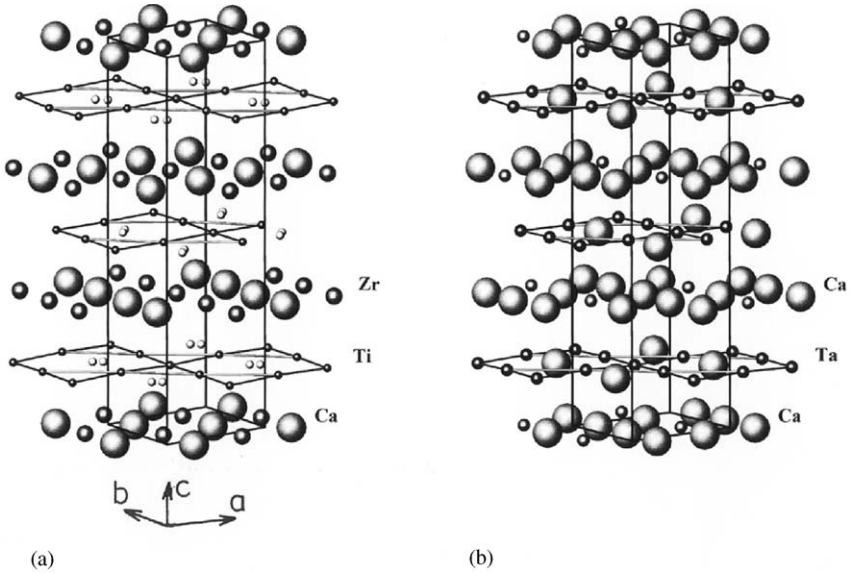

Fig. 1. Ordering of cubic close-packed metal atom layers in (a) 3T zirconolite and (b) 3T $Ca_2Ta_2O_7$ weberite-type.

10.7 wt% ThO_2 and 6.6 wt% Al_2O_3. These values are in reasonable agreement with the electron microprobe analyses given in the Experimental section.

The polyhedral bond lengths for 3T zirconolite are given in Table 4. The spread of bond distances and the mean values for the 5, 6, 7 and 8-coordinated sites are generally in very good agreement with the corresponding values in the 2M polytype [9]. The Ti site $M(4)$, has a low average bond distance of 1.93 Å, consistent with this site containing the major portion of the Al. The bond lengths for the AlO_4 tetrahedron, at site $M(5)'$ are longer by $\sim$0.1 Å than usually reported for tetrahedral Al. However, it is likely that there is local adjustment of the relevant oxygen atoms to adopt to the different coordination requirements of Ti, Zr in $M(5)$ and Al in $M(5)'$. This is supported by the relatively large U values for the relevant oxygen atoms, O(1), O(2) and O(4) reported in Table 2.

3.2. 3T calcium tantalate

The metal atom ordering in 3T calcium tantalate is shown in Fig. 1(b). It is consistent with other calcium tantalate polytypes in comprising alternate (001) layers ($=(111)_{\text{fluorite}}$) of composition Ta_3Ca and Ca_3Ta. The Ta_3Ca layers have HTB-type octahedral articulation of TaO_6 octahedra with Ca atoms in the centers of hexagonal rings, taking up hexagonal bipyramidal coordination which includes two short Ca–O distances to oxygen atoms O(2) above and below the rings (see the bond lengths for $M(5)$ in Table 4). The Ca_3Ta layers have kagome nets of Ca atoms in distorted cubic coordination with TaO_6 octahedra in the centers of the hexagonal rings such that all polyhedra share edges. Polyhedral diagrams of the two layer types are given in Fig. 1 of Ref. [5].

Unlike the fluoride weberite polytypes, $Na_2M^{2+}M^{3+}F_7$, for which the particular polytype stacking is characterized by the relative orientations of $[M^{2+}F_5]$ chains in successive HTB layers [2], the tantalates do not have mixed small-cation valency and thus cannot be distinguished in this way. An alternative classification can, however, be readily made based on the mode of corner linking of the isolated TaO_6 in the Ca_3Ta layers with the octahedra in the adjacent Ta_3Ca layers. In all weberite polytypes the isolated MX_6 octahedron shares only four of its 6 vertices with octahedra in the adjacent layers. The two non-bridging vertices can have a *cis* or *trans* configuration, and the different polytypes are distinguished by the sequence of *cis* and *trans* octahedra [2,6]. In 3T $Ca_2Ta_2O_7$ each of the three Ca_3Ta layers has a *cis* configuration of the TaO_6, with a different *cis* pair of oxygen atoms in each layer. For comparison, in the fluoride weberites, the 2O polytype has a *trans* configuration of its unique $M^{3+}F_6$ octahedron, the 2M has a *cis* configuration, and the 4M polytype has an alternation of *cis* and *trans* $M^{3+}F_6$ in successive large-cation layers [2]. 6T $Ca_2Ta_2O_7$ also has an alternation of *cis* and *trans* octahedra, with all three possible orientations of each [6].

3.3. 4M calcium tantalate

The 4M phase is the third calcium tantalate polytype to be characterized with fluorite-like cubic close packing of the metal atoms. A number of other polytypes have been characterized in which the *fcc* packing is periodically twinned on $(111)_{\text{fluorite}}$ to give mixed

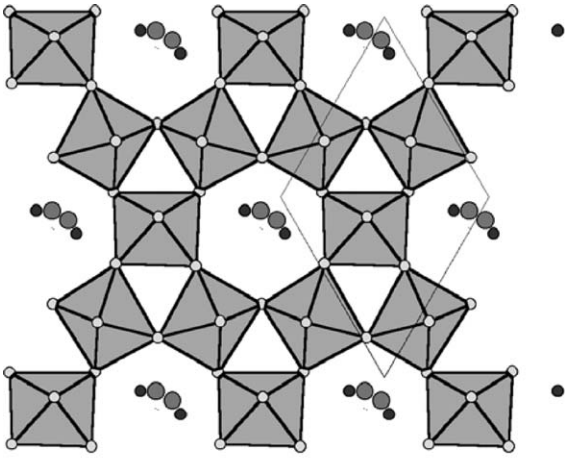

(a)

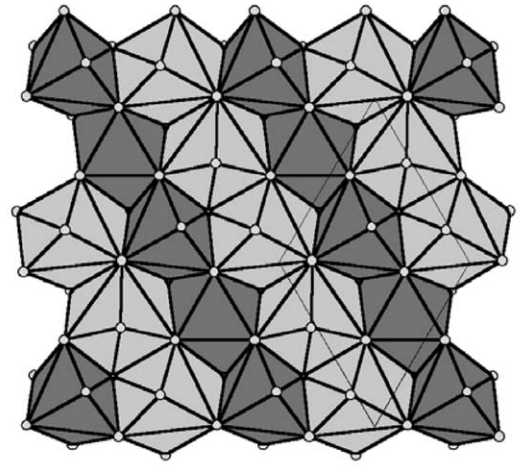

(b)

Fig. 2. Polyhedral (001) layers in 3T zirconolite. (a) HTB layer. Small circles are Al, larger circles are Ti. Unit cell outline shown. (b) Large-cation layer. Light shaded polyhedra are CaO_8 distorted cubes and dark shaded polyhedra are ZrO_7 mono-capped octahedra.

Table 4
Comparison of polyhedral bond distances for 3T zirconolite and 3T weberite (calcium tantalate)

	3T zirconolite		3T weberite
	Ca cube		*Ca cube*
M(1)–O(3)	2.395(6) × 2		2.713(9) × 2
M(1)–O(2)	2.408(6) × 2		2.445(8) × 2
M(1)–O(4)	2.469(6) × 2		2.727(7) × 2
M(1)–O(6)	2.511(7) × 2		2.459(6) × 2
	Ca cube		*Ta octahedron*
M(2)–O(3)	2.409(6) × 2		2.088(6) × 2
M(2)–O(2)	2.415(6) × 2		1.920(6) × 2
M(2)–O(5)	2.472(7) × 2		1.970(6) × 2
M(2)–O(1)	2.472(7) × 2		
	Zr 7–coord.		*Ca cube*
M(3)–O(3)	2.053(5)		2.528(8)
M(3)–O(5)	2.110(5)		2.701(9)
M(3)–O(6)	2.116(5)		2.296(6)
M(3)–O(7)	2.127(6)		2.706(7)
M(3)–O(2)	2.177(6)		2.419(8)
M(3)–O(6)	2.330(7)		2.354(6)
M(3)–O(5)	2.366(7)		2.726(8)
M(3)–O(1)			2.815(7)
	Ti octahedron		*Ta octahedron*
M(4)–O(7)	1.915(8) × 2		1.989(7) × 2
M(4)–O(6)	1.918(5) × 2		1.996(6) × 2
M(4)–O(4)	1.954(8) × 2		2.014(7) × 2
	5-coord	*4-coord.*	*Ca hex. bipyramid*
M(5)–O(2)	1.769(7)	1.83(2)	2.160(6) × 2
M(5)–O(2)	1.801(7)	1.84(2)	
M(5)–O(4)	1.893(7)	1.98(2)	2.507(8) × 2
M(5)–O(4)	2.243(9)		
M(5)–O(1)	2.278(9)	1.87(2)	2.886(6) × 2
M(5)–O(7)			2.549(8) × 2
	Ti octahedron		*Ta octahedron*
M(6)–O(1)	1.919(9)		1.959(7)
M(6)–O(7)	1.951(8)		1.968(7)
M(6)–O(5)	1.956(6)		1.993(6)
M(6)–O(4)	1.969(7)		1.955(7)
M(6)–O(1)	1.975(9)		1.974(7)
M(6)–O(3)	2.001(6)		1.968(6)

cubic-hexagonal stacking of the metal atom layers [5,6,18]. A polyhedral representation of the 4M structure is shown in Fig. 3. The polytype layer stacking is characterized by the sequence *cis–cis–cis–trans* of non-bridging oxygen atoms associated with the octahedra in successive Ca_3Ta layers. A summary of the polyhedral bond length ranges and mean values are given in Table 5, where the *cis* and *trans* Ca_3Ta layers are identified. The mean Ca–O and Ta–O bond length ranges are narrow and fall within the ranges observed for other calcium tantalate polytypes [6,18].

Refined site occupancies for the metal atom sites in the 4M polytype are given in Table 3. These site occupancies correspond to calculated analyses of 19.4 wt% CaO, 76.4 wt% Ta_2O_5, 1.8 wt% ZrO_2 and 2.4 wt% Nd_2O_3, are in reasonable agreement with the microprobe analyses given in the Experimental section. The highest level of Zr substitution occurs in the Ta(42) site in the *trans* Ca_3Ta layer. The highest level of Nd substitution is in the Ca(4) hexagonal bipyramidal site in the *trans* Ca_3Ta layer.

3.4. Structure relations for zirconolite and weberite polytypes

The 3T zirconolite structure is closely related to that of the 2M polytype [9]. Both polytypes have an alternation of Ti_4 and Ca_2Zr_2 layers. In the 2M polytype there are only two orientations of the Ca_2/Zr_2 chains, at 120° to one another in successive Ca_2Zr_2 layers, whereas

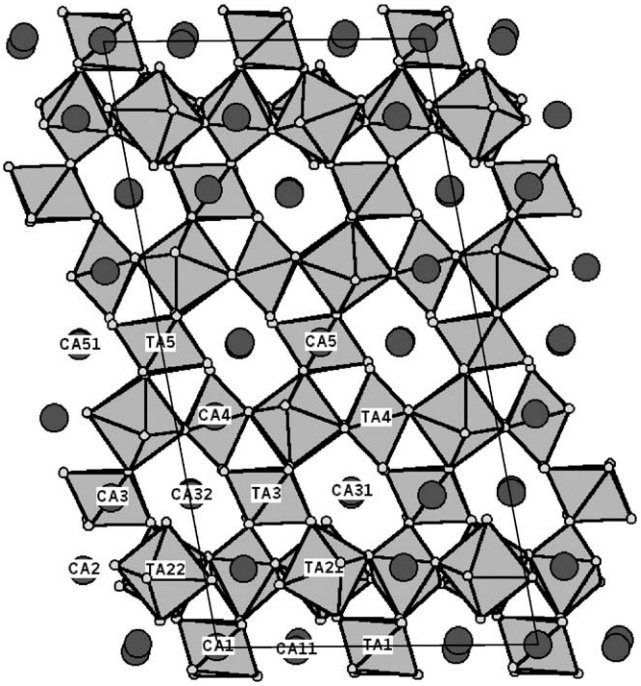

Fig. 3. Polyhedral representation of the structure for 4M $Ca_2Ta_2O_7$ weberite-type, viewed along [010]. The *a*-axis is horizontal. Filled circles are Ca atoms. Metal atom labelling shown, consistent with Table 3.

Table 5
Polyhedral distances for 4M $Ca_2Ta_2O_7$

Atom	$\langle M$–O$\rangle$	*M*–O range	Layer type
Ca(1)	2.61	2.50–2.71	*Cis*–Ca_3Ta
Ta(1)	1.99	1.89–2.10	*Cis*–Ca_3Ta
Ca(11)	2.58	2.33–2.95	*Cis*–Ca_3Ta
Ta(2)	1.97	1.94–2.03	Ta_3Ca
Ca(2)	2.54	2.08–2.96	Ta_3Ca
Ta(21)	1.97	1.95–1.99	Ta_3Ca
Ta(22)	1.98	1.95–2.00	Ta_3Ca
Ca(3)	2.56	2.25–2.82	*Cis*–Ca_3Ta
Ta(3)	2.00	1.90–2.09	*Cis*–Ca_3Ta
Ca(31)	2.59	2.40–2.88	*Cis*–Ca_3Ta
Ca(32)	2.57	2.28–2.76	*Cis*–Ca_3Ta
Ta(4)	1.99	1.97–2.03	Ta_3Ca
Ca(4)	2.54	2.14–2.89	Ta_3Ca
Ta(41)	1.97	1.94–2.00	Ta_3Ca
Ta(42)	1.98	1.95–2.01	Ta_3Ca
Ca(5)	2.56	2.25–2.85	*trans*–Ca_3Ta
Ta(5)	2.00	1.96–2.04	*trans*–Ca_3Ta
Ca(51)	2.60	2.37–2.86	*trans*–Ca_3Ta

in the 3T polytype, all three possible orientations occur as shown in Fig. 1(a). The 3T and 2M polytypes differ in the disposition of small cations in the hexagonal rings in the HTB layers. The 2M polytype has a Ti atom displaced from the center of the ring to occupy a 5-coordinated site with trigonal pyramidal symmetry. The 3T polytype has partial occupancy of the same type of 5-coordinated site but in addition has partial occupancy by Al of a 4-coordinated site with distorted tetrahedral coordination. A similar situation pertains in 3O zirconolite where Ti is 5-coordinated and Fe is 4 coordinated [10]. All zirconolites have this feature of a statistical distribution of small cations in sites that are displaced from the center of the hexagonal ring.

The 3T and 2M polytypes are the only true zirconolite polytypes, which retain an alternation of Ti_4 and Ca_2Zr_2 layers. The 3O zirconolite polytype [10] has a complex HTB layer comprising 3-octahedra wide [001] bands of HTB-type corner-connected TiO_6 octahedra with Fe atoms in the hexagonal rings, alternating with chains of 7-coordinated Zr (Ti_2–TiFe–Ti_2–Zr_2), while the large-cation layer has an alternation of [001] chains given by Ca_2–Zr_2–Ca_2–TiFe with substantial substitution of lanthanides and Th in the Ca sites. In addition the 3O polytype has two separate orientations of these layers, perpendicular to [101] and [10–1] of the orthorhombic cell. The fourth reported zirconolite polytype, 4M [12], which is stabilized by doping with Nd, is actually an ordered intergrowth of zirconolite and pyrochlore elements. There are two types of large-cation layers; a pyrochlore-type with ideal composition Ca_3Ti and a zirconolite-type, ideally Ca_2Zr_2. There is extensive Nd/Ca and Zr/Ti substitution in both layer types [12]. Ordered intergrowth of pyrochlore and weberite-type blocks also occurs, for example in the 4M tantalate polytype $Na_2Ta_2O_5F_2$ [19], and in 5M $Ca_2Ta_2O_7$ doped with $Sm_2Ti_2O_7$ [6]. However, intergrowth of zirconolite and weberite structure elements has not been reported.

A comparison of the atomic positions in the zirconolite and weberite 3T polytypes is facilitated by the use of the same labelling for equivalent atoms in the presentation of the atomic coordinates in Table 2. The largest coordinate changes in going from zirconolite to weberite are seen to be for *z* of O(1) ($\equiv$a shift of $\sim$1.2 Å along [001]) and for *y* of O(3) and O(5) (representing displacements of $\sim$0.7 Å). There are also large displacements of the small cations *M*(5) and *M*(5)′ (0.55 and 0.7 Å, respectively) from the center of the hexagonal ring in the HTB layer of zirconolite, to take up 5- and 4-coordination as discussed above. A further difference is that the metal atoms in the Ca_3Ta layers of the weberite phase are very close to co-planar, whereas the Zr atoms are displaced by $\pm$0.3 Å from the plane of the Ca atoms in the Ca_2Zr_2 layers in zirconolite. The displacements of successive Zr atoms in the Zr_2 chains are alternately in opposite directions parallel to [001].

The atomic coordinate changes from weberite-3T to zirconolite-3T are accompanied by a large contraction in the *c*-axis of zirconolite relative to weberite, given in Table 1. Relative to the parent cubic fluorite structure, zirconolite-3T undergoes a strong contraction along one

of the $\{111\}_{\text{fluorite}}$ axes ($c/\sqrt{2}a = 1.644$, cf. 1.732 for fluorite). A compression along one of the $\{111\}$ directions has been noted for other zirconolites [11]. In contrast, the weberite-type calcium tantalates are all expanded along one $\{111\}_{\text{fluorite}}$ axis. For example, $c/2\sqrt{2}a = 1.741$ for the 3T polytype and $3c^*/4\sqrt{2}a = 1.743$ for the 4M polytype. Valence sum calculations [20] for zirconolite-3T give values of $\sim$2.2 for Ca and 3.7 for Zr, so that the Ca–O bonds are in relative compression while the Zr–O bonds are under tension in the large-cation layers. In contrast, valence sum calculations for 3T and 4M calcium tantalate give values of 1.5–1.8 for Ca so the Ca–O bonds are under tension in the weberite polytypes.

The changes in polyhedral coordination resulting from the coordinate changes between weberite-3T and zirconolite-3T are given in Table 4. It is seen that the large displacement of O(1) is responsible for the main polyhedral changes. The O(1) displacement changes the coordination of the $M(3)$ site from 7 in zirconolite (Zr) to 8 in weberite (Ca), and the coordination of the $M(2)$ site from 8 in zirconolite (Ca) to 6 in weberite (Ta). Thus, rather than the Ca_2 chain being maintained in the two structures and the Zr_2 chain changing to a CaTa chain, the O(1) displacement changes the coordination of the metal atoms in both the Ca_2 and Zr_2 chains. Table 4 shows that the other polyhedral coordination changes result from displacements of O(1), O(4) and O(7), converting the coordination of the $M(5)$ site from 8 in weberite (Ca) to 5 and 4 in zirconolite (Ti and Al). The large displacements of O(3) and O(5) noted above do not lead to polyhedral coordination changes, but are associated with large changes in M–O bond lengths for $M(1)$, $M(2)$ and $M(3)$ as seen from Table 4.

The metal-centered polyhedral description of the zirconolite and weberite polytypes, as used above, is useful for depicting the structure/composition relationships in these phases. However, in terms of understanding their relationships to the fluorite structure, of which they are considered anion-deficient derivatives, it is more instructive to concentrate on the cubic close-packed metal atom arrays and the ordering of anions in the tetrahedral interstices. The use of anion-centered tetrahedra was used by Caro [21] for describing the structural differences between the A, B and C-type RE_2O_3 compounds. This approach has been extensively developed by O'Keeffe and Hyde [22] and Krivovichev and Filatov ([23] and references therein). For other than binary phases there is a fundamental difference between cation-centered polyhedra and anion-centered polyhedra. The cation-centered polyhedra usually have only one type of ligand, for example O or F and the charge distribution approximates to spherical. However, in ternary and higher phases the anions are surrounded by cations that can differ greatly in both size and charge, such as in the $Ca_2Ta_2O_7$ polytypes where O is surrounded by different combinations of Ta^{5+} and Ca^{2+}. This leads to very distorted coordinations for the anions. In the following discussion we are concerned primarily with the topology of the atomic arrangements but recognize that a detailed analysis of the differences between zirconolite and weberite polytypes needs to take account of the locally distorted environments of the anions.

In weberite-type $Ca_2Ta_2O_7$ polytypes, the cubic stacking of metal atom layers of composition Ca_3Ta alternating with Ta_3Ca gives rise to eight different tetrahedral environments for the oxygen atoms. The M_4O_7 composition requires that one of the eight tetrahedral interstitial sites is unoccupied. The unoccupied site can be predicted from simple valency considerations. The tetrahedral compositions are Ca_3Ta ($\times 2$), Ta_2Ca_2 ($\times 4$) and Ta_3Ca ($\times 2$). The formal Pauling valencies ($\sum v/\text{CN}$) for an oxygen atom at the centers of these tetrahedra are 1.58, 2.17 and 2.75. The required valency for oxygen can be achieved in the first case, where the valency is under-saturated, by the oxygen moving towards the highly charged Ta^{5+} cations. In the second case, the formal valency is close to 2 and only small displacements are required. However, for the two Ta_3Ca tetrahedra, the oxygen is highly over-saturated and the large displacement required to satisfy the charge requirement for oxygen cannot be achieved within the tetrahedra. Thus both of the Ta_3Ca tetrahedral sites are candidates for the oxygen vacancy and a compromise is established as illustrated in Fig. 4.

Fig. 4 shows that the two Ta_3Ca tetrahedra share a common edge. In fluorite, both of these sites would be occupied by anions. In $Ca_2Ta_2O_7$, one anion is removed and the other relocates to the adjacent octahedral site of composition Ca_4Ta_2 that shares faces with the two Ta_3Ca tetrahedra (forming a compound interstitial site in the form of a bisdisphenoid). The anion locates close to the Ta–Ta edge of the octahedron so that it has four nearest neighbors in the form of an elongated tetrahedron of composition Ta_2Ca_2. A complete set of occupied tetrahedral sites between a pair of Ca_3Ta and Ta_3Ca layers in $Ca_2Ta_2O_7$ is shown in Fig. 5(b). The anion occupying the octahedral interstitial site, O(1) for 3T $Ca_2Ta_2O_7$, is shown as a sphere.

In zirconolite, ideally $CaZrTi_2O7$, the corresponding eight metal atom tetrahedra have compositions Ca_2ZrTi ($\times 2$), $CaTiZr_2$ ($\times 2$), $CaTi_3$ ($\times 2$) and $ZrTi_3$ ($\times 2$). The formal Pauling valencies for an anion at the center of these tetrahedra are 1.74, 2.06, 2.25 and 2.57. The first six tetrahedra require only small displacements to achieve the valency requirements of the interstitial oxygen atoms. The oxygen vacancy occurs in one of the over-saturated $ZrTi_3$ interstitial sites. These two sites differ in that one of them involves three Ti atoms from the HTB net and the other involves two Ti atoms from

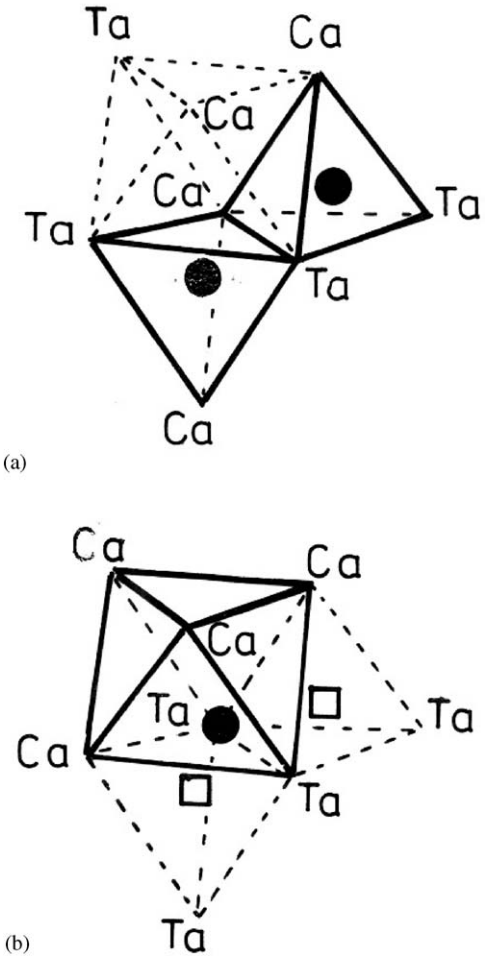

Fig. 4. Interstitial sites in the close-packed metal atom array in 3T $Ca_2Ta_2O_7$. (a) occupation of edge-shared pairs of Ca_2Ta_2 tetrahedra by oxygen (filled circles). The adjacent Ca_3Ta_3 octahedral interstitial site is shown by the dotted lines. (b) Edge-shared pairs of Ta_3Ca tetrahedra contain oxygen vacancies (squares). The oxygen atom re-locates to the adjacent Ca_4Ta_2 octahedral interstitial site.

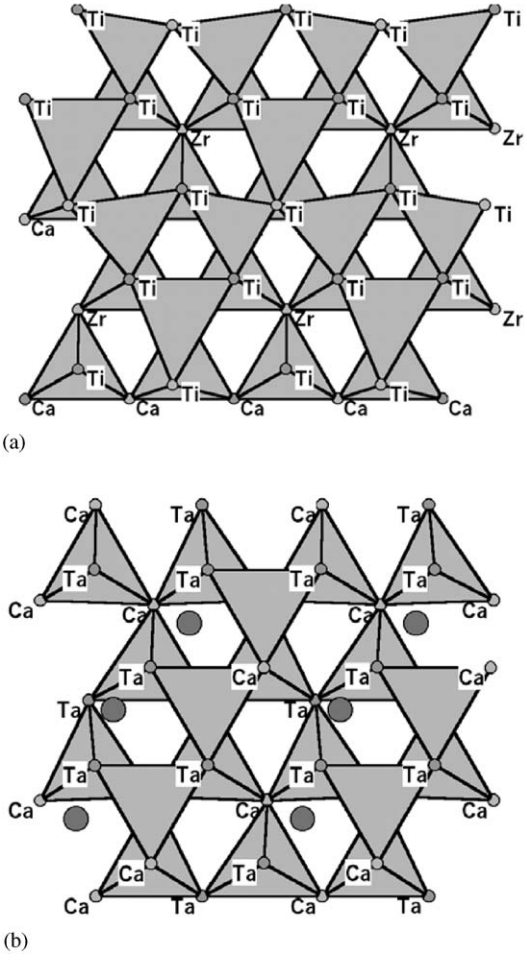

Fig. 5. Arrangements of anion-centered tetrahedra in (a) zirconolite and (b) $Ca_2Ta_2O_7$ weberite-type. The circles represents oxygen atoms in octahedral interstices, see Fig. 4(b).

the HTB net plus the Ti atom in the hexagonal ring. The latter has much greater flexibility to move to satisfy the oxygen valence requirements and so the anion vacancy occurs in the former tetrahedron. The arrangement of OM_4 tetrahedra between the Ti_4 and Ca_2Zr_2 layers of zirconolite is illustrated in Fig. 5(a).

Only zirconolite can be strictly described as an anion-deficient fluorite derivitive, because it retains both the cubic close packing of the metal atoms, and the ordering of anions and anion vacancies in the tetrahedral interstices of the metal atom framework. In weberite the topolology of edge-shared anion-centered tetrahedra is broken by location of one of the anions in an adjacent octahedral interstice. Pyrochlore is more closely related to zirconolite than to weberite in preserving both the cubic packing of metals and the ordering of anions in the tetrahedral interstices.

Acknowledgments

We thank Peter Fielding for the synthesis of 3T zirconolite, Gary Fallon for the single-crystal data collections and Colin MacRae for help with the microprobe analyses.

References

[1] A. Bystrom, Ark. Kemi Mineral. Geol. 18B (10) (1944) 7.
[2] O. Yakubovich, V. Urusov, W. Massa, G. Frenzen, D. Babel, Z. Anorg. Allg. Chem. 619 (1993) 1909–1919.
[3] O. Knop, G. Demazeau, P. Hagenmuller, Can. J. Chem. 58 (1980) 2221–2224.
[4] J. Reading, C.S. Knee, M.T. Weller, J. Mater. Chem. 12 (2002) 2376–2382.
[5] I.E. Grey, R.S. Roth, G. Mumme, L.A. Bendersky, D. Minor, Mater. Res. Soc. Symp. Proc. 547 (1999) 127–138.
[6] I.E. Grey, R.S. Roth, J. Solid State Chem. 150 (2000) 167–177.
[7] P. Bayliss, F. Mazzi, R. Munno, T.J. White, Mineral. Mag. 53 (1989) 565–569.

[8] Y.A. Pyatenko, Z.V. Pudovkina, Kristallografiya 9 (1964) 98.
[9] B.M. Gatehouse, I.E. Grey, R.J. Hill, H.J. Russell, Acta Crystallogr. Sect. B 37 (1981) 306–312.
[10] F. Mazzi, R. Munno, Am. Mineral. 68 (1983) 262–276.
[11] K.L. Smith, G.R. Lumpkin, Defects and processes in the solid state: geoscience applications, In: J.N. Boland, J.D. Fitzgerald (Eds.), Developments in Petrology, Vol. 14, The McLaren Volume, Elsevier, Amsterdam, 1993, pp. 401–422.
[12] A.A. Coelho, R.W. Cheary, K.L. Smith, J. Solid State Chem. 129 (1997) 346–359.
[13] G.R. Lumpkin, K.L. Smith, M.G. Blackfird, R. Giere, C.T. Williams, Micron 25 (1994) 5.
[14] G.M. Sheldrick, SHELXL, University of Gottingen, Germany, 1997.
[15] H.J. Rossell, J. Solid State Chem. 99 (1992) 52–57.
[16] W. Verscharen, D. Babel, J. Solid State Chem. 24 (1978) 405–421.
[17] H.J. Rossell, J. Solid State Chem. 99 (1992) 38–51.
[18] I.E. Grey, R.S. Roth, W.G. Mumme, J. Planes, L. Bendersky, C. Li, J. Chenavas, J. Solid State Chem. 161 (2001) 274–287.
[19] M. Vlasse, J.-P. Chaminade, J.-C. Massies, M. Pouchard, J. Solid State Chem. 12 (1975) 102–109.
[20] N.E. Brese, M. O'Keeffe, Acta Crystallogr. Sect. B 47 (1991) 192–197.
[21] P.E. Caro, J. Less-Common Metals 16 (1968) 367–377.
[22] M. O'Keeffe, B.G. Hyde, Struct. Bonding 61 (1985) 77–144.
[23] S.V. Krivovichev, S.K. Filatov, Acta Crystallogr. Sect. B 55 (1999) 664–676.